Prediction of the dynamic oscillation threshold in a clarinet model with a linearly increasing blowing pressure : Influence of noise

Baptiste Bergeot, André Almeida, Christophe Vergez, Bruno Gazengel

Prediction of the dynamic oscillation threshold in a clarinet model with a linearly increasing blowing pressure : Influence of noise

B. Bergeot[a,*], A. Almeida[a], C. Vergez[b], B. Gazengel[a]

[a] LUNAM Université, Université du Maine, UMR CNRS 6613, Laboratoire d'Acoustique, Avenue Olivier Messiaen, 72085 Le Mans Cedex 9, France

[b] Laboratoire de Mécanique et Acoustique (LMA, CNRS UPR7051), 31 Chemin Joseph Aiguier, 13402 Marseille Cedex 20, France

Abstract

This paper presents an analysis of the effects of noise and precision on a simplified model of the clarinet driven by a variable control parameter.

In a previous work [5], the dynamic oscillation threshold of a simplified model of a clarinet is obtained analytically. In the present article, the sensitivity of the dynamic threshold on precision is analyzed as a stochastic variable introduced in the model. A new theoretical expression is given for the dynamic thresholds in presence of the stochastic variable, providing a fair prediction of the thresholds found in finite-precision simulations. The dynamic thresholds are found to depend on increase rate and are independent on the initial value of the parameter, both in simulations and in theory.

Keywords: Musical acoustics, Clarinet-like instruments, Iterated maps, Dynamic Bifurcation, Bifurcation delay, Transient processes, Noise, Finite precision.

1. Introduction

A previous article by the authors [5] analysed the behavior of a simplified model of a clarinet when one of its control parameters (the blowing pressure) increases linearly with time. The oscillations corresponding to the production of sound start at a much higher threshold of the blowing pressure than the one obtained in a static parameter case. The dynamic threshold was described by an analytical expression, predicting that it does not depend on the increase rate of the blowing pressure (within the limits of the theory, i.e. slow enough increases), but that it is very sensitive to the starting value of the linear increase.

These results are reproduced by simulations of the model, but only when very high precisions are used in the simulations (Fig. 10 in [5]). Running the simulation with the normal double-precision of a CPU results in much lower thresholds, although higher than the static ones. In contrast with the theory and simulations using high precision, the threshold depends on the rate of increase of the parameter, but doesn't depend on the starting value of the blowing pressure.

The aim of the present article is to estimate the dynamic bifurcation threshold in simulations performed with finite precision. The effect of finite numerical precision in simulations is modeled as an ad hoc additive white noise with uniform distribution. This hypothesis is tested in section 3. In section 4, a mathematical relation is derived for the behavior of the model affected with noise, following a general method given by Baesens [3]. The resulting theoretical expression of the dynamic oscillation threshold is compared to numerical simulations and its range of validity is discussed. The clarinet model and major results from [5] are first briefly recalled in section 2.

A table of notation is provided in table 1 .

2. Dynamic oscillation threshold of the clarinet model without noise

2.1 Clarinet model

The instrument is divided into two functional elements: the exciter and the resonator. The exciter of the clarinet is the reed-mouthpiece system described by a nonlinear characteristics relating the instantaneous values of the flow $u(t)$ across the reed entrance to the pressure difference $\Delta p(t) = p_m(t) - p(t)$ between the mouth of the musician and the clarinet mouthpiece [10, 9]. The reed is simplified into an ideal spring without damping or inertia. The resonator is approximated to a straight cylinder,

*Corresponding author, baptiste.bergeot@univ-lemans.fr

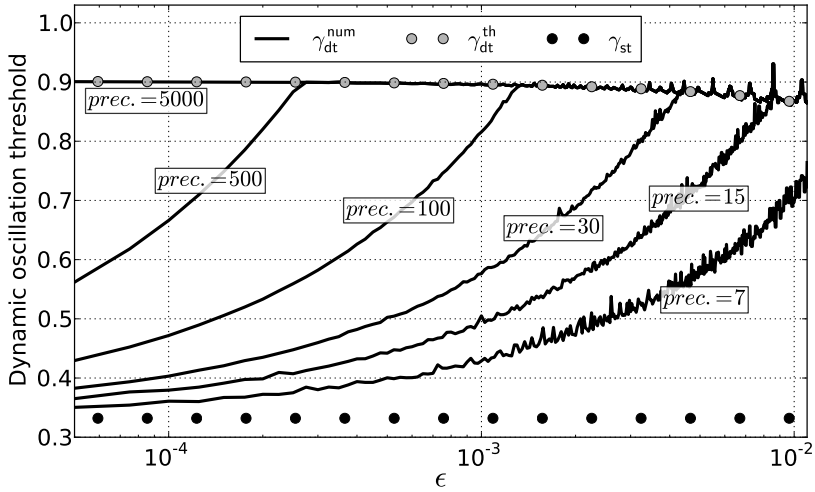

Figure 1: Graphical representation of γ_{dt}^{num} for different precisions (prec. = 7, 15, 30, 100, 500 and 5000) with respect to the slope ϵ and for $\gamma_0 = 0$. Results are also compared to analytical *static* and *dynamic* thresholds: γ_{st} and γ_{dt}^{th}.

Table 1: Table of notation. All quantities are dimensionless.

Table of Notation	
G	iterative function
γ	musician mouth pressure (control parameter)
ζ	control parameter related to the opening of the embouchure at rest
p^+	outgoing wave
p^-	incoming wave
p^{+*}	non-oscillating static regime of p^+ (fixed points of the function G)
ϕ	invariant curve
w	difference between p^+ and ϕ
ϵ	increase rate of the parameter γ
σ	level of the white noise
γ_{st}	static oscillation threshold
γ_{dt}	dynamic oscillation threshold
γ_{dt}^{th}	theoretical estimation of the dynamic oscillation threshold of the clarinet model without noise or in "deterministic" situation
$\hat{\gamma}_{dt}^{th}$	theoretical estimation of the dynamic oscillation threshold of the noisy clarinet model in "sweep-dominant" situation
$\tilde{\gamma}_{dt}^{th}$	general theoretical estimation of the dynamic oscillation threshold of the noisy clarinet model, both for a "sweep-dominant regime" or a "deterministic regime"
γ_{dt}^{num}	dynamic oscillation threshold calculated on numerical simulations

described by its reflection function $r(t)$. Assuming perfect reflexions at the open of the resonator (no radiation losses) and ignoring viscous and thermal losses the reflexion function becomes a simple delay with sign inversion.

The solutions $p(t)$ and $u(t)$ of the model depend on two control parameters: γ representing the blowing pressure and ζ related to the opening of the embouchure at rest. In this work, the control parameter ζ is always constant and equal to 0.5. Using the variables $p^+ = \frac{1}{2}(p+u)$ and $p^- = \frac{1}{2}(p-u)$ (outgoing and incoming pressure waves respectively) instead of the variables p and u, the state of the system can be calculated at regular intervals $\tau = 2L/c$, the round trip time of the sound wave along the resonator. With these assumptions, the nonlinear system becomes an iterated map [12, 13, 11] :

$$p_n^+ = G\left(p_{n-1}^+, \gamma\right). \tag{1}$$

The function G can be written explicitly for $\zeta < 1$ (see Taillard et al. [15]). When the control parameter γ is constant, for low values of γ the solution of eq. (1) stabilises at an equilibrium point, and for a critical value γ_{st} a flip bifurcation occurs leading to a periodic regime that corresponds to sound production.

2.2 Dynamic bifurcation

For a linearly increasing control parameter γ, eq. (1) is replaced by eq. (2a) and (2b) :

$$\begin{cases} p_n^+ = G\left(p_{n-1}^+, \gamma_n\right) & \text{(2a)} \\ \gamma_n = \gamma_{n-1} + \epsilon. & \text{(2b)} \end{cases}$$

The theory derived in section 4 requires that the parameter γ increase slowly, hence ϵ is considered arbitrarily small ($\epsilon \ll 1$).

Because of the time variation in the control parameter γ, the bifurcation point corresponding to the appearance of the oscillations is shifted from the *static oscilla-*

tion threshold γ_{st} [6] to the *dynamic oscillation threshold* γ_{dt} [5]. The difference $\gamma_{dt}-\gamma_{st}$ is called the *bifurcation delay* [3, 7]. The previous article by the authors [5] provides an analytical study of the dynamic flip bifurcation of the clarinet model (i.e. system (2)) based on applications of dynamic bifurcation theory proposed by Baesens [3]. The main focus of this work is on the properties of the dynamic oscillation threshold, recalled hereafter.

The trajectory of the system in the phase space (here constituted of a single variable p^+) through time is called the *orbit*. The dynamic oscillation threshold is defined as the value of γ for which the orbit escapes from the neighborhood of the *invariant curve* $\phi(\gamma,\epsilon)$. This definition is different from the one used in [5] where the dynamic threshold was defined as the value of gamma for which the orbit starts to oscillate.

The invariant curve is the nonoscillating solution of the system (2). It plays the role of an attractor for variable parameters similarly to the role of the fixed point in a static case. The invariant curve is written as a function of the parameter, invariant under the mapping (2) and thus satisfying the following equation:

$$\phi(\gamma,\epsilon) = G\big(\phi(\gamma-\epsilon,\epsilon),\gamma\big). \tag{3}$$

The procedure to obtain the theoretical estimation γ_{dt}^{th} of the dynamic oscillation threshold is as follows: a theoretical expression of the invariant curve is found for a particular (small) value of the increase rate ϵ (i.e. $\epsilon \ll 1$). The system (2) is then expanded into a first-order Taylor series around the invariant curve and the resulting linear system is solved analytically. Finally, γ_{dt}^{th} is derived from the analytic expression of the orbit.

The dynamic oscillation threshold γ_{dt}^{th} is defined by [5]:

$$\int_{\gamma_0+\epsilon}^{\gamma_{dt}^{th}+\epsilon} \ln\left|\partial_x G\big(\phi(\gamma'-\epsilon),\gamma'\big)\right| d\gamma' = 0, \tag{4}$$

where γ_0 is the initial value of γ (i.e. the starting value of the linear ramp). Two important remarks can be made on this expression (Fig. 6 of [5]):

- γ_{dt}^{th} does not depend on the slope of the ramp ϵ, provided that ϵ is small enough,
- γ_{dt}^{th} depends on the initial value γ_0 of the ramp.

These properties are also observed in numerical simulations with very high precision.

2.3 Problem statement

The above theoretical predictions converge towards the observed simulation results for very high numerical precision (typically when thousands of digits are considered

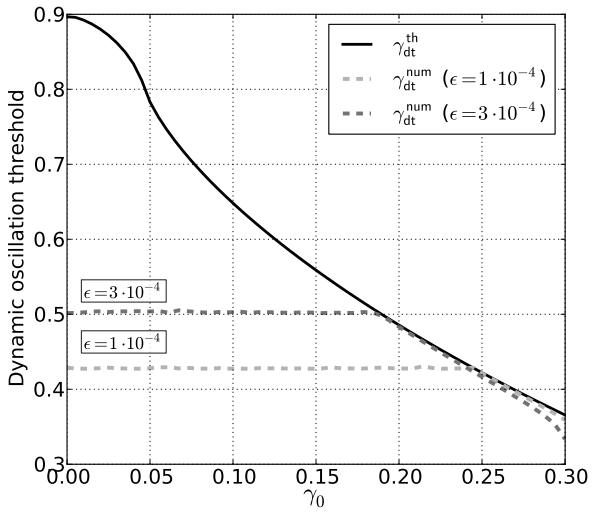

(a) Numerical precision is fixed (prec. = 50). γ_{dt}^{num} is computed for $\epsilon = 10^{-4}$ and $3\cdot10^{-4}$.

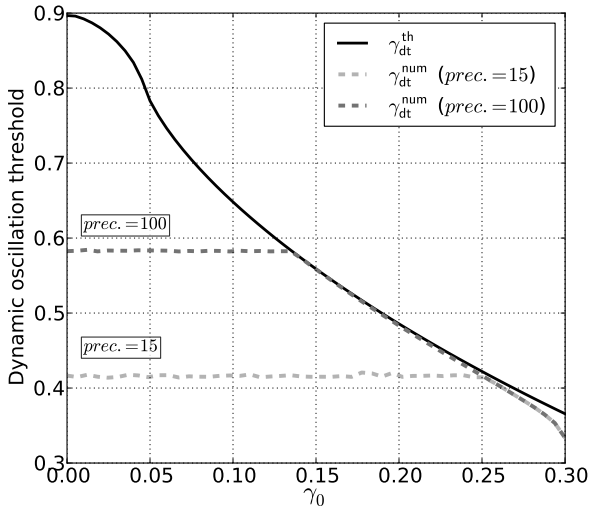

(b) The increase rate of γ is fixed ($\epsilon = 3\cdot10^{-4}$). γ_{dt}^{num} is computed for numerical precisions equal to 15 and 100.

Figure 2: Plot of γ_{dt} as a function of the initial condition γ_0. Solid lines are the theoretical prediction γ_{dt}^{th} calculated from equation (4). Dashed line represent the values γ_{dt}^{num}.

in the simulation). Figure* 1 shows that for the usual double-precision of CPUs (around 15 decimals), theoretical predictions of the dynamic bifurcation point γ_{dt}^{th} are far from thresholds estimated on the numerical simulation results γ_{dt}^{num}. In particular, the numerical bifurcation point γ_{dt}^{num} depends on the slope ϵ, in contrast with the

*This is a plot similar to figure 10 of [5]. The only difference is that the bifurcation point γ_{dt}^{num} estimated on the simulation results is here defined by the point where the orbit leaves the neighborhood of the invariant curve. The motivation for this choice will appear clearly in section 3 where random variables are considered.

theoretical predictions γ_{dt}^{th}. Moreover, figure 2 reveals that for a low numerical precision (though even significantly higher than typical precisions used in numerical simulations), the dependance of the bifurcation point on the initial value γ_0 is lost over a wide range of γ_0.

The minimum precision for which round-off errors do not affect the behavior of the system depends on the relative magnitude of the slope ϵ, the precision and the initial condition γ_0. Indeed, figure 1 shows that, beyond a certain value of ϵ all curves join the one with highest precision. Curves for even higher precisions would overlap, allowing to conclude that they are representative of an infinitely precise case. As shown in figure 2, for given values of ϵ and of the numerical precision beyond a certain value of γ_0, the theoretical result γ_{dt}^{th} allows to obtain a good prediction of the bifurcation delay.

As a conclusion, the theoretical results obtained in [5] are not able to predict the behavior of numerical simulations carried out at usual numerical precision. The aim of this paper is to show how the numerical precision can be included in a theoretical model that correctly describes numerical simulations. Firstly, it is shown that the model computed with a finite precision behaves similarly to the model with an ad-hoc additive white noise. This is done in the next section. Then, using theoretical results proposed by Baesens [3], a modified expression describing the behavior of the model affected by noise (section 4).

3. Finite precision versus additive white noise

Differences between theoretical predictions and numerical simulations highlighted in the previous section are due to round-off errors that accumulate for finite precisions. The aim of this section is to verify that round-off errors of the computer can be modeled as an additive independent and identically distributed random variable (referred to as an additive white noise). This result is used in section 4 to derive theoretical predictions of the dynamic bifurcation point γ_{dt}.

Two numerical results are compared. The first is the simulation of the system (2) using a numerical precision pr_1 (hereafter referred as a *finite precision case*). The second one (hereafter referred as a *noisy case*) is the simulation of the following stochastic system of difference equations:

$$\begin{cases} p_n^+ = G\left(p_{n-1}^+, \gamma_n\right) + \xi_n & \text{(5a)} \\ \gamma_n = \gamma_{n-1} + \epsilon, & \text{(5b)} \end{cases}$$

where ξ_n is a uniformly distributed stochastic variable with an expected value equal to zero (i.e. $\mathbb{E}[\xi_n] = 0$) and a level σ defined by:

$$\mathbb{E}[\xi_m \xi_n] = \sigma^2 \delta_{mn}, \tag{6}$$

where δ_{mn} is the Kronecker delta. The definition of the expected value $\mathbb{E}$ is provided in [14]. For comparison with the finite precision case the noise level σ is equal to 10^{-pr_1}.

The bifurcation point γ_{dt}^{num} estimated on the simulations is defined as the value of γ for which the orbit leaves the neighborhood of the invariant curve. Since the mean value of the white noise ξ_n is zero, the relevant quantity to study is the mean square deviation of the orbit from the invariant curve. Therefore, γ_{dt}^{num} is reached when:

$$\sqrt{\mathbb{E}\left[w_n^2\right]} = \epsilon, \tag{7}$$

where $w_n = p_n^+ - \phi(\gamma_n, \epsilon)$ describes the distance between the actual orbit and the invariant curve. Among other possible criteria, the condition (7) is chosen because it is also used in the analytical calculation made in section 4.

To simplify the notation, in the rest of the document the invariant curve will be noted $\phi(\gamma)$. Its dependency on parameter ϵ is no longer explicitly stated.

In figures 3 and 4, γ_{dt}^{num} is estimated in the finite precision case and in the noisy case. In both cases an average is made on w_n^2 obtained in 20 different simulations. Then,

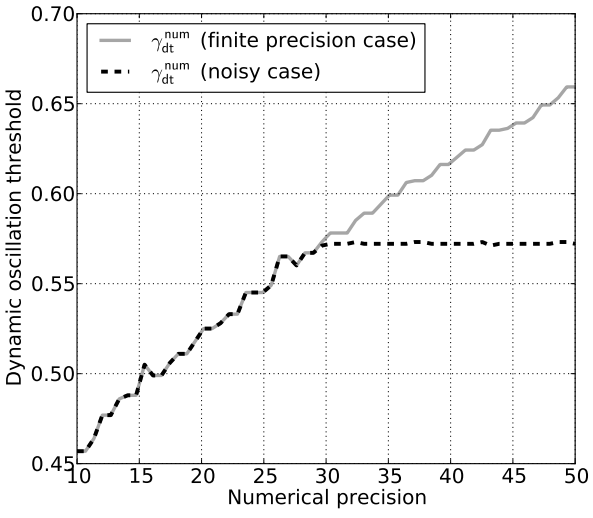

Figure 3: Comparison of the dynamic threshold γ_{dt}^{num} obtained in numerical simulations of a noiseless (2) clarinet model and one (5) where a noise of level $\sigma = 10^{-30}$ is introduced. The dynamic threshold of oscillation obtained over an average of 20 runs is plotted against the precision used in the simulations, showing that beyond a precision of about σ, the system affected with noise is insensitive to the precision.

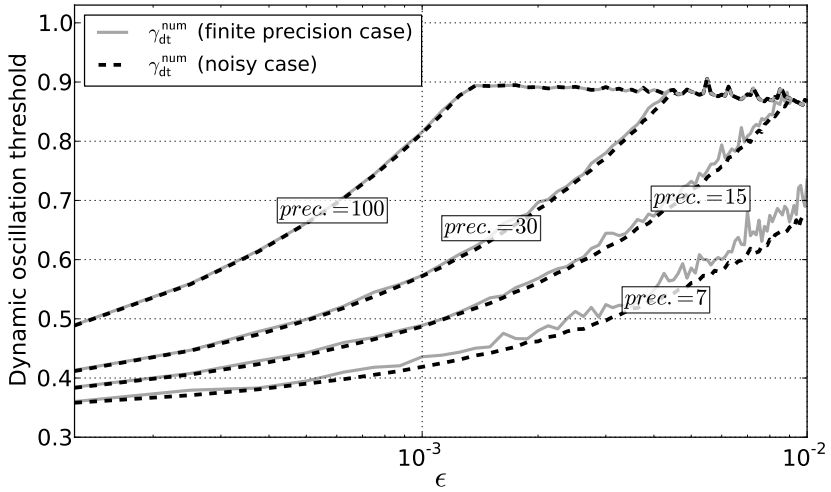

Figure 4: Comparison between γ_{dt}^{num} computed for *finite precision cases* and for *noisy cases*. For both cases and for each value of ϵ we compute the average of the signals $w_n = p_n^+ - \phi(\gamma_n)$ obtained over 20 runs. Then, γ_{dt}^{num} is calculated on the resulting signal. The numerical precisions used to simulate the finite precision cases are 7, 15, 30 and 100 decimal digits. $\gamma_0 = 0$.

γ_{dt}^{num} is calculated on the mean signal using equation (7).

In figure 3, γ_{dt}^{num} is plotted with respect to the numerical precision for which systems (2) and (5) are simulated. The noise level σ of the noisy case is equal to 10^{-30}. Before the numerical precision becomes equal to $-\log_{10}\sigma = 30$, the noise level is smaller than round-off errors of the computer. In these situations, the thresholds computed in finite precision case and in noisy case are equals. For numerical precisions larger than 30, γ_{dt}^{num} computed on system (5) is constant because the influence of the noise overrides that of the round-off errors of the computer. Therefore, to avoid the influence of the numerical precision, the system (5) is now simulated using a precision $pr_2 \gtrsim 2pr_1$, we choose $pr_2 = 2pr_1$.

Figure 4 confirms that the kind of noise introduced in the stochastic system can correctly describe a finite precision. Indeed, with the exception of the smallest precision ($pr_1 = 7$), the curves are nearly superimposed. Hence, in the next section, the stochastic system (5) is studied theoretically in order to predict results of numerical simulations of system (2) with finite precision.

4. Analytical study of the noisy dynamic case

4.1 General solution of the stochastic clarinet model

This section introduces a formal solution of the stochastic model that is valid when the orbit is close to the invariant curve. Function G in equation (5a) is expanded into a first-order Taylor series around the invariant curve. Using the variable $w_n = p_n^+ - \phi(\gamma_n)$, the system (5) becomes:

$$\begin{cases} w_n = w_{n-1}\partial_x G\big(\phi(\gamma_n - \epsilon), \gamma_n\big) + \xi_n & \text{(8a)} \\ \gamma_n = \gamma_{n-1} + \epsilon. & \text{(8b)} \end{cases}$$

The solution of equation (8a) is [4]:

$$w_n = w_0 \prod_{k=1}^{n} \partial_x G\big(\phi(\gamma_k - \epsilon), \gamma_k\big) + \sum_{k=1}^{n} \xi_k \prod_{m=k+1}^{n} \partial_x G\big(\phi(\gamma_m - \epsilon), \gamma_m\big), \quad (9)$$

where w_0 is the initial value of w_n.

Because the additive white noise ξ_n has a zero-value mean, as in section 3, the relevant indicator is the mean square deviation of the orbit from the invariant curve: $\sqrt{\mathbb{E}[w_n^2]}$. Equation (9) squared becomes:

$$\begin{aligned} w_n^2 = &\left(w_0 \prod_{k=1}^{n} \partial_x G\big(\phi(\gamma_k - \epsilon), \gamma_k\big) \right)^2 \\ &+ \left(\sum_{k=1}^{n} \xi_k \prod_{m=k+1}^{n} \partial_x G\big(\phi(\gamma_m - \epsilon), \gamma_m\big) \right)^2 \\ &+ 2w_0 \sum_{k=1}^{n} \left(\prod_{j=1}^{n} \partial_x G\big(\phi(\gamma_j - \epsilon), \gamma_j\big) \right) \xi_k \\ &\times \prod_{m=k+1}^{n} \partial_x G\big(\phi(\gamma_m - \epsilon), \gamma_m\big). \quad (10) \end{aligned}$$

Averaging has no effect on the first term of the right-hand side of equation (10) because the stochastic variable

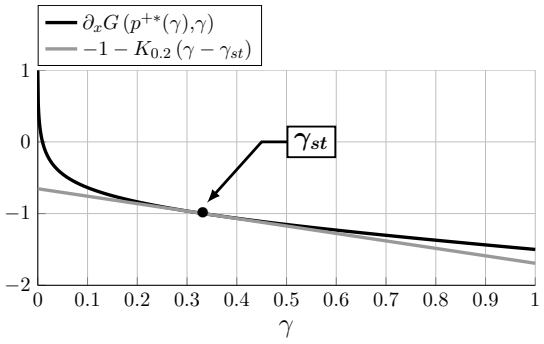

(a) $\zeta = 0.2$

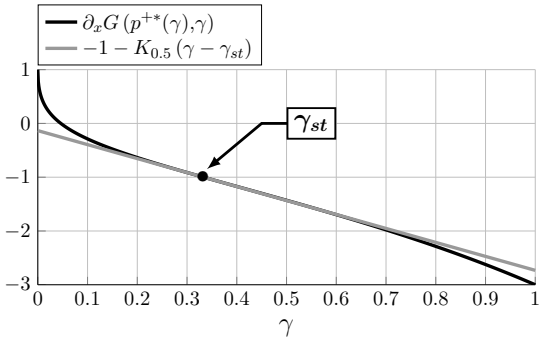

(b) $\zeta = 0.5$

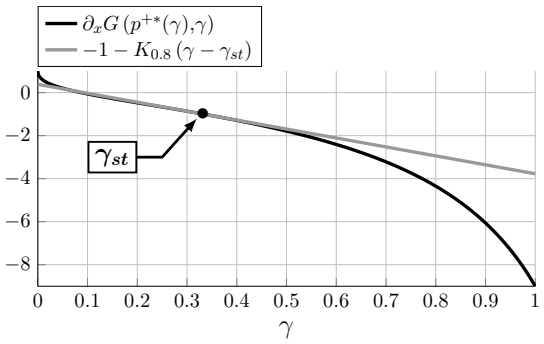

(c) $\zeta = 0.8$

Figure 5: Graphical representation of $\partial_x G\big(p^{+*}(\gamma),\gamma\big)$ and its tangent function $-1-K\big(\gamma-\gamma_{st}\big)$ around the static oscillation threshold for $\zeta = 0.2$, 0.5 and 0.8.

ξ_n is not present. Using eq. (6), the average of the second term is simplified to:

$$\sigma^2 \sum_{k=1}^{n} \left(\prod_{m=k+1}^{n} \partial_x G\big(\phi(\gamma_m - \epsilon), \gamma_m\big) \right)^2. \tag{11}$$

Because $\mathbb{E}[\xi_n] = 0$, the average of the third term of the right-hand side of equation (10) is also equal to zero. Using the fact that a product can be expressed as an exponential of a sum of logarithms, the final expression of $\mathbb{E}\big[w_n^2\big]$ is given by:

$$\mathbb{E}\big[w_n^2\big] = \underbrace{w_0^2 \left(\exp\left(\sum_{k=1}^{n} \ln\left|\partial_x G\big(\phi(\gamma_k - \epsilon), \gamma_k\big)\right| \right) \right)^2}_{A_n}$$
$$\underbrace{+\sigma^2 \sum_{k=1}^{n} \left(\exp\left[\sum_{m=k+1}^{n} \ln\left|\partial_x G\big(\phi(\gamma_m - \epsilon), \gamma_m\big)\right| \right] \right)^2}_{B_n}. \tag{12}$$

Finally, using Euler's approximation, sums are replaced by integrals and the expressions of A_n and B_n become:

$$A_n \approx w_0^2 \exp\left(\int_{\gamma_0+\epsilon}^{\gamma_n+\epsilon} 2\ln\left|\partial_x G\big(\phi(\gamma'-\epsilon),\gamma'\big)\right| \frac{d\gamma'}{\epsilon} \right), \tag{13}$$

$$B_n \approx \frac{\sigma^2}{\epsilon} \int_{\gamma_0+\epsilon}^{\gamma_n+\epsilon} \left\{ \exp\left(\int_{\gamma+\epsilon}^{\gamma_n+\epsilon} 2\ln\left|\partial_x G\big(\phi(\gamma'-\epsilon),\gamma'\big)\right| \frac{d\gamma'}{\epsilon} \right) \right\} d\gamma. \tag{14}$$

A_n corresponds to the precise case studied in [5] which leads to the theoretical estimation γ_{dt}^{th} of the dynamic oscillation threshold for the system without noise (cf. equation (4)). B_n is the contribution due to the noise, which will be considered in the remaining of this section.

A first glance on equations (13) and (14) allows to explain observation made in Section 2.3. Indeed, comparing the expressions of A_n and B_n, it possible to distinguish [3, 2] two operating regimes, which, for a given values of w_0, depends on ϵ, σ and γ_0:

- $A_n \gg B_n$ **(deterministic regime)**

  In this case the noise does not affect the bifurcation delay and the dynamic oscillation threshold can be determined by eq. (4).

- $A_n \ll B_n$ **(sweep-dominant regime)**

  In this case, the bifurcation delay is affected by the noise. This regime is studied in the following section.

In Section 2.3, figures 1 and 2 represent two different cases distinguished by the parameter values: in certain areas of the figures, the dynamic bifurcation threshold does not depend on ϵ but depends on γ_0, while in other areas the dynamic bifurcation threshold depends on ϵ but is not dependent on γ_0. This observation may be interpreted as the existence of the two regimes detailed above: a **sweep-dominant regime** and a **deterministic regime**. The transition between the two regimes occurs abruptly as observed in figures 1 and 2.

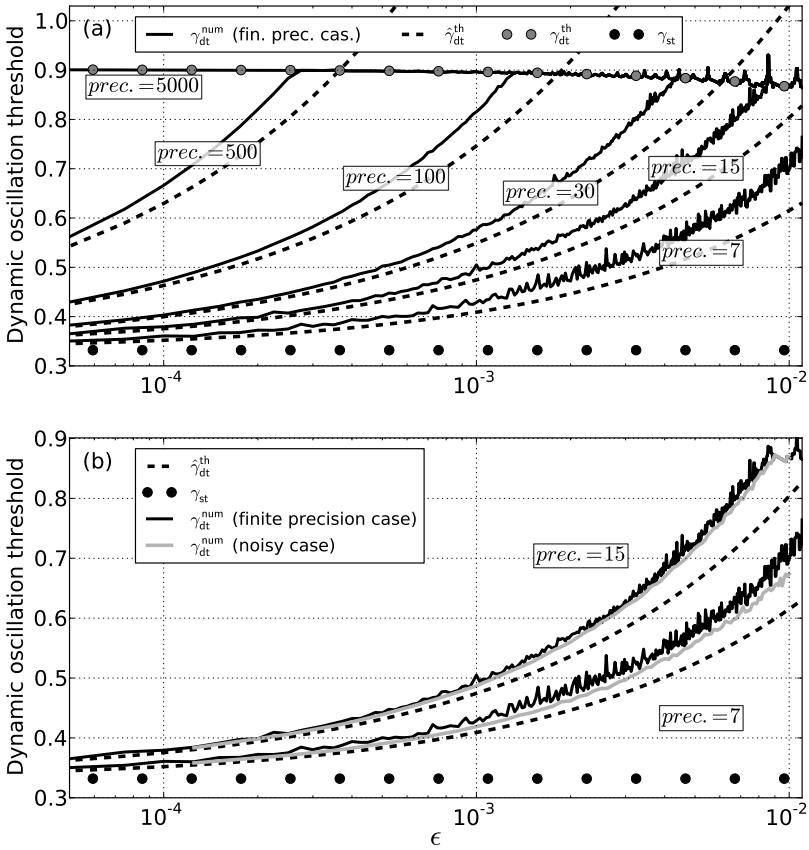

Figure 6: Graphical representation of γ_{dt}^{num} for different precisions (prec. = 7, 15, 30, 100, 500 and 5000) with respect to the slope ϵ and for $\gamma_0 = 0$. Results are also compared to analytical *static* and *dynamic* thresholds: γ_{st}, γ_{dt}^{th} and $\hat{\gamma}_{dt}^{th}$. (a) γ_{dt}^{num} and only *finite precision cases* are represented. (b) Both *finite precision cases* and *noisy cases* are represented for prec. = 7 and 15.

4.2 Theoretical expression of the dynamic oscillation threshold of the stochastic model

The next step is to find an approximate expression of the standard deviation $\sqrt{\mathbb{E}\left[w_n^2\right]}$ for the sweep-dominant regime. In this regime, the term A_n is negligible with respect to the contribution B_n due to the noise, i.e. $\sqrt{\mathbb{E}\left[w_n^2\right]} \approx \sqrt{B_n}$. The purpose is to obtain a statistical prediction of the dynamic oscillation threshold for the stochastic system, hereafter referred as $\hat{\gamma}_{dt}^{th}$.

It is assumed that $\epsilon \ll 1$, which implies that the invariant curve $\phi(\gamma)$ and the curve $p^{+*}(\gamma)$ of the fixed points in eq. (1) are close [5], and allows the approximation:

$$\partial_x G\big(\phi(\gamma-\epsilon),\gamma\big) \approx \partial_x G\big(p^{+*}(\gamma),\gamma\big). \tag{15}$$

Moreover, because of the noise, the bifurcation delay is expected to occur earlier, so that the dynamic oscillation threshold γ_{dt} is assumed to be close[†] to the static oscillation threshold γ_{st}. The term $\partial_x G\big(p^{+*}(\gamma),\gamma\big)$ is then expanded in a first-order Taylor series around the static oscillation threshold γ_{st}:

$$\partial_x G\big(p^{+*}(\gamma),\gamma\big) \approx \underbrace{\partial_x G\big(p^{+*}(\gamma_{st}),\gamma_{st}\big)}_{\triangleq -1\text{: flip bifurcation}} + \big(\gamma-\gamma_{st}\big)\underbrace{\partial_{xy} G\big(p^{+*}(\gamma_{st}),\gamma_{st}\big)}_{\text{noted} -K}, \tag{16}$$

finally we have:

$$\partial_x G\big(p^{+*}(\gamma),\gamma\big) \approx -1 - K\big(\gamma-\gamma_{st}\big), \tag{17}$$

which is used in equation (14). Figure 5 shows the com-

[†]This hypothesis could be questioned because according to figures 1 and 2, even in the presence of noise, the bifurcation delay can be big. However, this hypothesis is required to carry out following calculations.

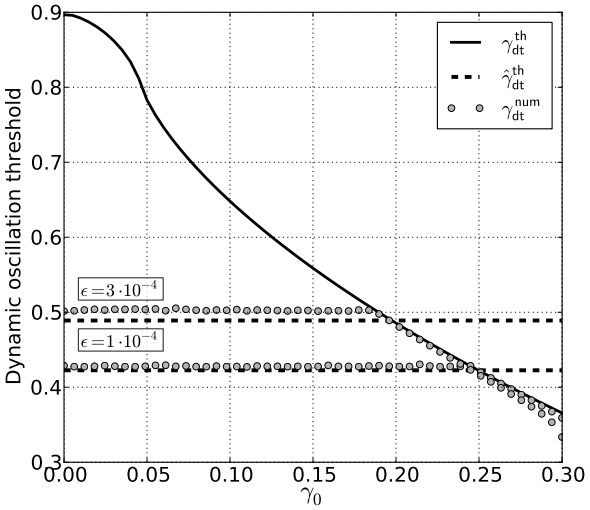

(a) Numerical precision is fixed (prec. = 50). $\hat{\gamma}_{dt}^{th}$ and γ_{dt}^{num2} are computed for $\epsilon = 10^{-4}, 6\cdot10^{-4}$.

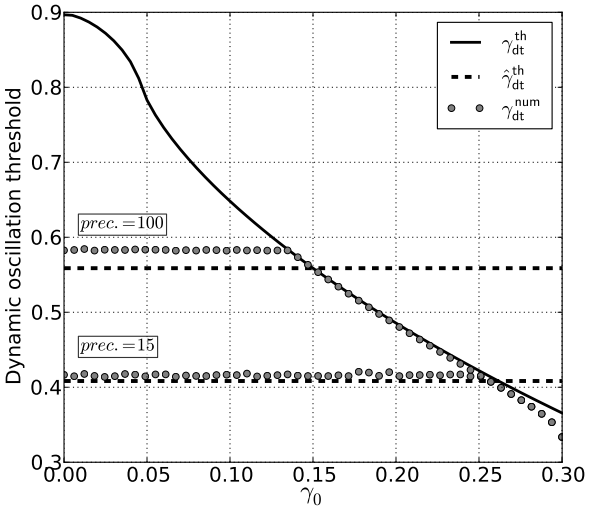

(b) The increase rate of γ is fixed ($\epsilon = 3\cdot10^{-4}$). $\hat{\gamma}_{dt}^{th}$ and γ_{dt}^{num2} are computed for numerical precisions equal to 15 and 100.

Figure 7: Comparison between theoretical prediction of dynamic oscillation threshold (without noise: γ_{dt}^{th} and with noise: $\hat{\gamma}_{dt}^{th}$) and the dynamic threshold γ_{dt}^{num} computed on numerical simulations for finite precision case. Variable are plotted with respect to the initial condition γ_0.

parison between $\partial_x G\left(p^{+*}(\gamma),\gamma\right)$ and its tangent function $-1-K\left(\gamma-\gamma_{st}\right)$ around the static oscillation threshold for $\zeta = 0.2$, 0.5 and 0.8. The linearisation appears as a good approximation of the function in a wide domain of γ around the static oscillation threshold γ_{st}. For large values of the control parameter ζ (cf. fig. 5(c)) the linear approximation is valid over a narrower range of γ.

Using expression (17) the integral

$$I_1 = \int_{\gamma+\epsilon}^{\gamma_n+\epsilon} 2\ln\left|\partial_x G\left(\phi(\gamma'-\epsilon),\gamma'\right)\right| \frac{d\gamma'}{\epsilon}, \tag{18}$$

contained in the expression (14) of B_n becomes:

$$I_1 = \frac{2K}{\epsilon}\int_{\gamma+\epsilon}^{\gamma_n+\epsilon}\left(\gamma'-\gamma_{st}\right)d\gamma' = \frac{K}{\epsilon}\left[\left(\gamma'-\gamma_{st}\right)^2\right]_{\gamma+\epsilon}^{\gamma_n+\epsilon}. \tag{19}$$

The small correction ϵ in the domain of integration can be neglected since $\epsilon \ll 1$. Therefore, we obtain:

$$\begin{aligned} I_1 &= \frac{K}{\epsilon}\left[\left(\gamma'-\gamma_{st}\right)^2\right]_{\gamma}^{\gamma_n} \\ &= \frac{K}{\epsilon}\left[\left(\gamma_n-\gamma_{st}\right)^2-\left(\gamma-\gamma_{st}\right)^2\right]. \end{aligned} \tag{20}$$

By combining equations (14) and (20), B_n is now written as:

$$\begin{aligned} B_n \approx\ & \frac{\sigma^2}{\epsilon}\int_{\gamma_0+\epsilon}^{\gamma_n+\epsilon}\exp\left(\frac{K}{\epsilon}\left[\left(\gamma_n-\gamma_{st}\right)^2-\left(\gamma'-\gamma_{st}\right)^2\right]\right)d\gamma' \\ &= \frac{\sigma^2}{\epsilon}\exp\left(\frac{K}{\epsilon}\left(\gamma_n-\gamma_{st}\right)^2\right) \\ &\quad\times \underbrace{\int_{\gamma_0+\epsilon}^{\gamma_n+\epsilon}\exp\left(-\frac{K}{\epsilon}\left(\gamma'-\gamma_{st}\right)^2\right)d\gamma'}_{I_2}. \end{aligned} \tag{21}$$

The function which appears in the integral I_2 is a Gaussian function with standard deviation

$$\nu = \sqrt{\frac{\epsilon}{2K}}. \tag{22}$$

Integral I_2 is then [8]:

$$I_2 = \left[\frac{1}{2}\sqrt{\frac{\pi\epsilon}{K}}\,\mathrm{erf}\left(\sqrt{\frac{K}{\epsilon}}\left(\gamma'-\gamma_{st}\right)\right)\right]_{\gamma_0}^{\gamma_n}, \tag{23}$$

where $\mathrm{erf}(x)$ is the error function. The initial condition γ_0 is supposed to be much lower than the static threshold γ_{st}, so that equation (23) can be written:

$$I_2 = \frac{1}{2}\sqrt{\frac{\pi\epsilon}{K}}\left[\mathrm{erf}\left(\sqrt{\frac{K}{\epsilon}}\left(\gamma_n-\gamma_{st}\right)\right)+1\right]. \tag{24}$$

The dependence on the initial condition γ_0 is now lost.

Since $\epsilon \ll 1$, for $\gamma_n > \gamma_{st}$ the error function quickly becomes equal to 1 and the integral I_2 is simplified to $I_2 = \sqrt{\frac{\pi\epsilon}{K}}$. Finally the expression of B_n is:

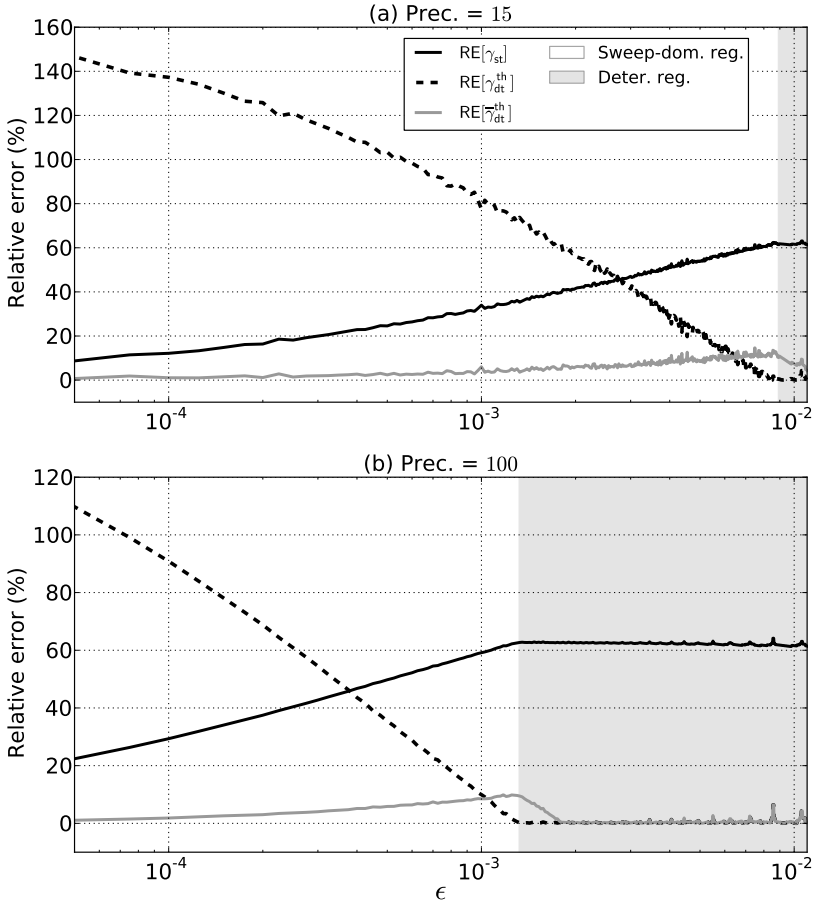

Figure 8: Relative errors: $RE[\gamma_{st}]$, $RE\left[\gamma_{dt}^{th}\right]$ and $RE\left[\tilde{\gamma}_{dt}^{th}\right]$ for numerical precisions equal to 15 (a) and 100 (b).

$$B_n \approx \frac{\sigma^2}{\sqrt{\epsilon}}\sqrt{\frac{\pi}{K}}\exp\left(\frac{K}{\epsilon}\left(\gamma_n-\gamma_{st}\right)^2\right). \tag{25}$$

From equation (25) it is possible to obtain the expression of $\sqrt{\mathbb{E}\left[w_n^2\right]} \approx \sqrt{B_n}$:

$$\sqrt{\mathbb{E}\left[w_n^2\right]} \approx \sigma\,\epsilon^{-1/4}\left(\frac{\pi}{K}\right)^{1/4}\exp\left(\frac{K}{2\epsilon}\left(\gamma_n-\gamma_{st}\right)^2\right). \tag{26}$$

The dynamic oscillation threshold $\hat{\gamma}_{dt}^{th}$ is defined [3, 2] as the value of γ_n for which the standard deviation $\sqrt{\mathbb{E}\left[w_n^2\right]}$ leaves the neighborhood of the invariant curve. More precisely, the bifurcation occurs when $\sqrt{\mathbb{E}\left[w_n^2\right]}$ becomes equal to the increase rate ϵ, as defined in eq. (7). Finally, using equation (26), we have:

$$\hat{\gamma}_{dt}^{th} = \gamma_{st} + \sqrt{-\frac{2\epsilon}{K}\ln\left[\left(\frac{\pi}{K}\right)^{1/4}\frac{\sigma}{\epsilon^{5/4}}\right]}, \tag{27}$$

which is the theoretical estimation of the dynamic oscillation threshold of the stochastic systems (5) (or of the system (2) computed using a finite precision) when it evolves in a sweep-dominant regime. The bifurcation delay is a by-product of eq. (27) since it is simply $\hat{\gamma}_{dt}^{th} - \gamma_{st}$.

The method presented in this section is based on a first-order Taylor expansion of the system (5) around the invariant curve $\phi(\gamma_n)$, leading to the linear system (8). Using an asymptotic expansion of the error function it is possible to investigate the behavior of $\sqrt{B_n}$ before γ_n enters the neighborhood of the static oscillation threshold γ_{st}. This study allows to define the domain of validity of this linear approximation, as done by Baesens [3, 2]. This is $\sigma \gtrsim \sqrt{\epsilon}$. This condition is respected in this work since $\sigma = 10^{-pr}$ with $7 \leq pr \leq 5000$ and $8.10^{-5} \leq \epsilon \leq 10^{-2}$. More details on obtaining the domain of validity are given in Appendix A.

4.3 Discussion

In figure 6, $\hat{\gamma}_{dt}^{th}$ defined by equation (27) is plotted against the increase rate ϵ. It is compared with γ_{dt}^{num} for different values of the precision and for $\gamma_0 = 0$. In figure 6(a), γ_{dt}^{num} is represented for finite precision cases. The significant differences between finite precision cases and stochastic cases observed for prec. = 7 and 15 are shown in figure 6(b). The theoretical result $\hat{\gamma}_{dt}^{th}$ provides a good estimation of the dynamic oscillation threshold as long as the system remains in the sweep-dominant regime (with a better estimation when the bifurcation delay is small[‡]). Otherwise, γ_{dt}^{th} is a better approximation of γ_{dt}^{num}, as expected in the deterministic regime.

Figure 7 shows the comparison between $\hat{\gamma}_{dt}^{th}$ and γ_{dt}^{num} (only for finite precision cases) plotted against the initial condition γ_0. In figure 7(a), variables are plotted for several values of ϵ and for a fixed numerical precision. The opposite is done in figure 7(b). As in figure 6, $\hat{\gamma}_{dt}^{th}$ provides a good estimation of the dynamic oscillation threshold in the sweep-dominant regime, as well as γ_{dt}^{th} in the deterministic regime.

Finally, to predict theoretically the dynamic bifurcation threshold $\bar{\gamma}_{dt}^{th}$ of the stochastic system (5) (as well as of the system (2) when it is computed with a finite precision) the following procedure is proposed:

- compute the theoretical estimation $\hat{\gamma}_{dt}^{th}$ of the stochastic system through eq. (27)
- compute the theoretical estimation γ_{dt}^{th} of the system without noise through eq. (4)
- if $\hat{\gamma}_{dt}^{th} < \gamma_{dt}^{th}$ the system remains in the "sweep-dominant regime" and the dynamic threshold $\bar{\gamma}_{dt}^{th}$ is equal to $\hat{\gamma}_{dt}^{th}$, otherwise the "deterministic regime" is attained and the dynamic threshold $\bar{\gamma}_{dt}^{th}$ is equal to γ_{dt}^{th}.

Figure 8 compares the relative error RE of the three theoretical predictions of the oscillation threshold (γ_{st}, γ_{dt}^{th} and $\bar{\gamma}_{dt}^{th}$) with respect to γ_{dt}^{num}, as a percent value:

$$RE[X] = 100 \times \left(\frac{|\gamma_{dt}^{num} - X|}{\gamma_{dt}^{num}} \right), \tag{28}$$

where X takes successively the values of γ_{st}, γ_{dt}^{th} and $\bar{\gamma}_{dt}^{th}$.

For standard double-precision (fig. 8(a), prec.=15), the sweep-dominant regime is prevalent throughout most of the range of increase-rates studied in this article. Higher precisions (for instance prec.=100) imply the appearence of the deterministic-regime for lower increase-rates. In this case, $\bar{\gamma}_{dt}^{th}$ provides a better estimation of the oscillation threshold of the clarinet with a linearly increasing blowing pressure. Indeed, in situations represented in figure 8, $RE\left[\bar{\gamma}_{dt}^{th}\right]$ never exceeds 15% while $RE\left[\gamma_{st}\right]$ and $RE\left[\gamma_{dt}^{th}\right]$ can reach 60% and 145% respectively. At slightly lower values of ϵ than the limit between the two regimes, γ_{dt}^{th} still provides a better estimation of γ_{dt}^{num} than $\bar{\gamma}_{dt}^{th}$, a situation that occurs for all values of the precision, according to figure 6.

[‡]This is an expected result because of the initial assumption of a small bifurcation delay in the presence of noise, leading to first-order Taylor expansions γ_{st} in previous calculation (see *step one* in section 4.2).

5. Conclusion

In many situations, the finite precision used in numerical simulations of the clarinet system does not produce major errors in the final results that are sought. Such is the case, for instance, when estimating the amplitudes for a given regime.

However, when slowly increasing one of the control parameters, the distances between the state of the system and the invariant curve can become smaller than the round-off errors of the calculation, with dramatic effects on the time required to trigger an oscillation. In these cases, the inclusion of a stochastic variable in the theory allows to correctly estimate the threshold observed in simulations, which lies between the static and dynamic thresholds found for precise cases.

As a final remark, the present theoretical study is probably not restricted to describe numerical simulations. Indeed, the noise level σ measured in an artificially blown instrument is typically of the order of magnitude of 10^{-3}. The domain of validity of the results: $\sigma \gtrsim \sqrt{\epsilon}$ suggests that the comparison with experiment using blowing pressure with increase rates $\epsilon > 10^{-6}$, seems to be possible although the noise level usually increases with the pressure applied to the instrument.

Acknowledgements

This work was done within the framework of the project SDNS-AIMV "Systèmes Dynamiques Non-Stationnaires - Application aux Instruments à Vent" financed by *Agence Nationale de la Recherche* (ANR).

A. Limit of the linear calculation

The method presented in Section 4 is based on a first-order Taylor expansion of the system (5) around the invariant curve $\phi(\gamma_n)$ leading to define the linear system (8). Following Baesens [3, 2], we give here the upper bound of the domain of validity of this linear approximation.

Using equations (14) and (24), the expression B_n is given by:

$$B_n = \frac{\sigma^2}{2}\sqrt{\frac{\pi}{\epsilon K}}\exp\left(\frac{K}{\epsilon}\left(\gamma_n-\gamma_{st}\right)^2\right) \times\left[\operatorname{erf}\left(\sqrt{\frac{K}{\epsilon}}\left(\gamma_n-\gamma_{st}\right)\right)+1\right]. \quad (29)$$

We investigate the behavior of $\mathbb{E}\left[w_n^2\right]$ before γ_n enters in the neighborhood of the static oscillation threshold γ_{st}. More precisely, we compute an approximate expression of $\mathbb{E}\left[w_n^2\right]$ when $\gamma_n < \gamma_{st} - \nu$, where ν is defined by equation (22). To do this, the error function in equation (29) is expanded in a first-order asymptotic series [1] (the asymptotic expansion of the error function $\operatorname{erf}(x)$ for large negative x is recalled in Appendix B):

$$B_n = \frac{\sigma^2}{2}\sqrt{\frac{\pi}{\epsilon K}}\exp\left(\frac{K}{\epsilon}\left(\gamma_n-\gamma_{st}\right)^2\right) \times\left[-1-\frac{\exp\left(-\frac{K}{\epsilon}\left(\gamma_n-\gamma_{st}\right)^2\right)}{\sqrt{\frac{K\pi}{\epsilon}}\left(\gamma_n-\gamma_{st}\right)}+1\right], \quad (30)$$

which is simplified in:

$$B_n = -\frac{\sigma^2}{2K\left(\gamma_n-\gamma_{st}\right)}. \quad (31)$$

Using the explicit form of γ_n, solution of equation (2b):

$$\gamma_n = \epsilon\, n + \gamma_0, \quad (32)$$

and (31), we have:

$$\sqrt{B_n} = \frac{\sigma}{\sqrt{2K\epsilon}}\frac{1}{\sqrt{n_{st}-n}}, \quad (33)$$

where n_{st} is the iteration for which γ_{st} is reached.

Equation (33) means that when $\gamma_n < \gamma_{st} - \mu$, the standard deviation $\sqrt{\mathbb{E}\left[w_n^2\right]} \approx \sqrt{B_n}$ increases with the time (i.e. with n) like $1/\sqrt{n_{st}-n}$ to order $\sigma/\sqrt{\epsilon}$, and therefore remains small if $\sigma \ll \sqrt{\epsilon}$. Otherwise, if $\sigma \gtrsim \sqrt{\epsilon}$, the orbit of the series p_n^+ leaves the neighborhood of invariant curve $\phi(\gamma)$ before the static oscillation threshold is reached. In this case, linear calculation made in Section 4 is no longer valid.

B. Asymptotic expansion of error function

The asymptotic expansion of the error function $\operatorname{erf}(x)$ for large negative x ($x \to -\infty$) is [1]:

$$\operatorname{erf}(x) \approx -1 - \frac{\exp\left(-x^2\right)}{\sqrt{\pi}x} \times\left(1+\sum_{m=1}^{+\infty}(-1)^m\frac{1\cdot 3\ldots(2m-1)}{\left(2x^2\right)^m}\right) \quad (34)$$

References

[1] Abramowitz, M., Stegun, I.A.: Handbook of Mathematical Functions: with Formulas, Graphs, and Mathematical Tables, first edn. Dover books on mathematics. Dover Publications, Incorporated, New York (1964)

[2] Baesens, C.: Noise effect on dynamic bifurcations: The case of a period-doubling cascade. In: Dynamic Bifurcations, *Lecture Notes in Mathematics*, vol. 1493, pp. 107–130. Springer Berlin Heidelberg (1991)

[3] Baesens, C.: Slow sweep through a period-doubling cascade: Delayed bifurcations and renormalisation. Physica D **53**, 319–375 (1991)

[4] Bender, C.M., Orszag, S.A.: Advanced Mathematical Methods for Scientists and Engineers (International Series in Pure and Applied Mathematics), chap. 2 "Difference equations". Mcgraw-Hill College (1978). URL http://www.worldcat.org/isbn/007004452X

[5] Bergeot, B., Vergez, C., Almeida, A., Gazengel, B.: Prediction of the dynamic oscillation threshold in a clarinet model with a linearly increasing blowing pressure. Nonlinear Dynamics pp. 1–14 (2013). DOI 10.1007/s11071-013-0806-y. URL http://dx.doi.org/10.1007/s11071-013-0806-y

[6] Dalmont, J., Gilbert, J., Kergomard, J., Ollivier, S.: An analytical prediction of the oscillation and extinction thresholds of a clarinet. J. Acoust. Soc. Am. **118**(5), 3294–3305 (2005)

[7] Fruchard, A., Schäfke, R.: Sur le retard à la bifurcation. In: International conference in honor of claude Lobry (2007). URL http://intranet.inria.fr/international/arima/009/pdf/arima00925.pdf

[8] Gradshteyn, I.S., Ryzhik, I.M.: Table of Integrals, Series, and Products (7th Ed.). Academic Press, New York (1965)

[9] Hirschberg, A.: Aero-acoustics of wind instruments. In: Mechanics of musical instruments by

A. Hirschberg/ J. Kergomard/ G. Weinreich, vol. 335 of *CISM Courses and lectures*, chap. 7, pp. 291–361. Springer-Verlag (1995)

[10] Hirschberg, A., de Laar, R.W.A.V., Maurires, J.P., Wijnands, A.P.J., Dane, H.J., Kruijswijk, S.G., Houtsma, A.J.M.: A quasi-stationary model of air flow in the reed channel of single-reed woodwind instruments. Acustica **70**, 146–154 (1990)

[11] Kergomard, J.: Elementary considerations on reed-instrument oscillations. In: Mechanics of musical instruments by A. Hirschberg/ J. Kergomard/ G. Weinreich, vol. 335 of *CISM Courses and lectures*, chap. 6, pp. 229–290. Springer-Verlag (1995)

[12] Maganza, C., Caussé, R., Laloë, F.: Bifurcations, period doublings and chaos in clarinet-like systems. EPL (Europhysics Letters) **1**(6), 295 (1986)

[13] Mcintyre, M.E., Schumacher, R.T., Woodhouse, J.: On the oscillations of musical instruments. J. Acoust. Soc. Am. **74**(5), 1325–1345 (1983)

[14] Ross, S.M.: Introduction to Probability Models, 9ème édition, chap. 2 "Random variables". Academic Press (2006). URL http://www.worldcat.org/isbn/0125980558

[15] Taillard, P., Kergomard, J., Laloë, F.: Iterated maps for clarinet-like systems. Nonlinear Dyn. **62**, 253–271 (2010)